Great Basin Water Resources

Creating a Remote Sensing User-Interface to Support Water Resource and Wetland Management for Inland Lakes

Summer 2026 | Virtual
August 7th, 2026

Authors: Katie Bossert (Analytical Mechanics Associates), Sofia Garcia (Analytical Mechanics Associates), Dean Gelling (Analytical Mechanics Associates), Vivian Maneval (Analytical Mechanics Associates), Kayla Sundling (Analytical Mechanics Associates)

Abstract:
Saline terminal lakes across the Great Basin are rapidly shrinking due to increasing water demand, groundwater extraction, and climate change, threatening wetland ecosystems, biodiversity, regional economies, and public health. The Oregon Department of Water Resources and the Utah Department of Natural Resources, Division of Water Resources currently rely on field measurements and conventional GIS analyses to track changing lake and wetland conditions. Integrating satellite-based Earth observations into routine decision-making is limited by time constraints and the need for domain-specific expertise. To address this, we developed a user-friendly QGIS plugin that automates long-term monitoring of terminal lakes and surrounding wetlands using Google Earth Engine. The workflow utilizes Landsat 5, 7, 8, and 9 imagery (1985–2026) to generate composites, calculate the Normalized Difference Water Index, Normalized Difference Vegetation Index, Normalized Difference Moisture Index, and Land Surface Temperature, classifying land cover into open water, wetlands, and land. Classification thresholds were optimized against OPERA Dynamic Surface Water Extent, JRC Global Surface Water, Google Dynamic World, and the National Wetlands Inventory. Validation showed strong performance, with Intersection-over-Union values reaching 0.844 and 0.870 for open water at Lake Abert and the Great Salt Lake, respectively. These thresholds serve as reliable defaults but can be adjusted by the user through the plugin. The finalized plugin lets users visualize historical trends, generate land cover maps, and quantify changes in lake and wetland extent. By streamlining Earth observation analysis, the tool supports partner ecosystem management and long-term monitoring while lowering the technical barriers associated with satellite data processing.

Key Terms: Landsat, QGIS, terminal lakes, remote sensing, time-series analysis, wetland classification, NDVI, NDWI

Advisors: Sean Fleming (NASA Ames Research Center, Cal State University Monterey Bay), Timothy Mayer (NASA Marshall Space Flight Center, University of Alabama in Huntsville), Jeremy Rapp (Marshall Space Flight Center, University of Alabama in Huntsville)

Project Coordinator: Caiden Hartrich (Virtual)

1. Introduction

Saline terminal lakes within the Great Basin are unique ecosystems that deliver important socio-economic benefits, including mineral extraction, recreation, aquaculture, and public works (Frus et al., 2023; Moore, 2016). The terminal lakes also support surrounding wetlands, which provide habitats for native wildlife, especially migratory birds and aquatic vegetation (Akumu et al., 2010). However, these lakes have experienced significant shrinking over the past century, primarily driven by increasing water demand, groundwater extraction, and climate change (Hall et al., 2023). Because terminal lakes lack outlets, water loss occurs only through evaporation or groundwater seepage, making them especially vulnerable to hydrological imbalance (Herring et al., 2025). Historically, the interconnected network of terminal lakes within the Great Basin contributed to regional ecological resilience but now faces unprecedented challenges. Continued lake decline threatens biodiversity and human communities through reduced water availability, economic losses related to recreation and industry, and increased exposure to dust and associated public health risks (Herring et al., 2025). For example, the Great Salt Lake supports approximately 7,000 jobs and generates $2 billion in economic output annually, all of which are increasingly threatened by the declining lake levels (Frus et al., 2023).

Given the ecological and economic risks, consistent monitoring of saline lakes and surrounding wetlands is essential but often limited by the high cost of fieldwork, instrumentation, and long-term maintenance (Moore, 2016). Remote sensing products provide high-spatiotemporal resolution imagery that supports large-scale monitoring of surface waters while reducing cost and labor demands (Yulianto et al., 2022). Landsat satellite imagery can quantify surface water extent, vegetation cover, and soil status, all of which are important for lake and wetland management. A previous remote sensing study conducted by Hall et al. indicated substantial hydrological decline across the region from 2001 to 2021. For example, the researchers discovered Lake Abert dropped in surface-water elevation by more than 3.0 m, leaving 99% of the lakebed exposed in the summer of 2022, and the Great Salt Lake by approximately 1.84 m, reaching its lowest surface-water elevation ever recorded in 2021 (Hall et al., 2023).

We conducted this project in partnership with the Oregon Department of Water Resources, Surface Water Section (ODWR), and the Utah Department of Natural Resources, Division of Water Resources (UDWR). These agencies rely on accurate, defensible environmental data to inform management decisions, evaluate changing waterbody conditions, and provide transparent, science-based information to stakeholders. Currently, ODWR and UDWR rely on field measurements and GIS analyses. Integration of Earth observation data into management remains limited by challenges associated with accessing, processing, validating, and leveraging large datasets, making long-term monitoring time- and expertise-intensive. To address these limitations, this project develops a user-friendly remote sensing workflow that integrates satellite-derived environmental data into existing practices.

We focused on two terminal lakes and their surrounding wetlands within the Great Basin, a 209,163-square-mile (541,729-square-kilometer) watershed spanning portions of Nevada, Utah, California, Idaho, and Oregon. The study sites are Lake Abert in south-central Oregon and the Great Salt Lake in northern Utah (Figure 1). Project partners selected these lakes because of their ongoing water-management challenges, documented declines in surface water extent, and changes to adjacent wetlands over recent decades. Although far from the only at-risk lakes in the Great Basin, these two lakes are representative of broader challenges, and the framework developed in this project can be expanded to additional imperiled lakes in the region as identified by Herring et al. (2025) and potentially elsewhere.

Figure 1: Terminal Lakes in the Great Basin, USA: Lake Abert, Oregon, and the Great Salt Lake, Utah. The center map consists of the designated lakes of study and the Great Basin Region. The left and right maps provide a zoomed-in view of Lake Abert and the Great Salt Lake, respectively.

The study period extends from January 1985 through May 2026. Beginning in 1985 captures more than four decades of variability in lake extent, water conditions, and wetland presence. The period also spans multiple generations of Landsat satellites, useful in creating a consistent long-term time series. Landsat's 16-day revisit cycle (and 8-day revisit when Landsat 8 and Landsat 9 are combined) provides sufficient temporal resolution to accurately monitor fluctuations in water and vegetation while maintaining a high spatial resolution. Extending the analysis through May 2026 captures historical conditions, long-term change, and the most recent conditions relevant to current resource management.

We developed a QGIS plug-in with a user-friendly graphical user interface (GUI) to simplify deriving environmental indices from Landsat and to generate time series for water extent and wetland analysis at Lake Abert and the Great Salt Lake. We utilized Google Earth Engine (GEE) and Landsat 5 Thematic Mapper (TM), Landsat 7 Enhanced Thematic Mapper Plus (ETM+), Landsat 8 Operational Land Imager (OLI), and Landsat 9 OLI-2 imagery to analyze water extent and wetland extent. Spectral indices included the Normalized Difference Water Index (NDWI) for water coverage, the Normalized Difference Vegetation Index (NDVI) and Normalized Difference Moisture Index (NDMI) for vegetation analysis, and Land Surface Temperature (LST) as a derived thermal product (Al-Maliki et al., 2022; Ashok et al., 2021). This tool addresses the need for improved water and wetland monitoring to support basin-wide management strategies related to water allocation, water distribution, and wetland and ecosystem management.

2. Methodology

2.1 Data Acquisition

We acquired Landsat Collection 2, Tier 1, Level 2 surface reflectance imagery through GEE to generate spectral index visualizations and land classifications for Lake Abert and the Great Salt Lake. The plug-in automatically selects imagery from all operational Landsat satellites within the user-specified time period, pulling from the Landsat platforms provided in Table 1a. This automated workflow provides continuous image coverage from 1985 to 2026.

Table 1a
Earth Observations

Platform	Use	Date Range Used in GUI
Landsat 5 Thematic Mapper (TM)	Provided the temporal (16 days) and spatial (30 m) resolution needed for index calculation, land classification, and land surface temperature.	1985–2012
Landsat 7 Enhanced Thematic Mapper Plus (ETM+)	Provided the temporal (16 days) and spatial (30 m) resolution needed for index calculation, land classification, and land surface temperature.	1999–2012
Landsat 8 Operational Land Imager (OLI) & Thermal Infrared Sensor (TIRS)	Provided the temporal (16 days) and spatial (30 m) resolution needed for index calculation, land classification, and land surface temperature.	2013–2026
Landsat 9 Operational Land Imager 2 (OLI-2) & Thermal Infrared Sensor (TIRS-2)	Provided the temporal (16 days) and spatial (30 m) resolution needed for index calculation, land classification, and land surface temperature.	2021–2026

We used four reference datasets, provided in Table 1b, to calibrate and validate the NDWI, NDVI, and NDMI thresholds employed in the threshold-based land classification workflow for the two Great Basin study sites. For NDWI optimization, we utilized the NASA OPERA Dynamic Surface Water Extent from Harmonized Landsat and Sentinel-2 (DSWx-HLS) product and the Joint Research Centre (JRC) Global Surface Water Monthly History dataset. The DSWx-HLS product, obtained from NASA Earthdata, provides operational surface water classifications derived from harmonized Landsat and Sentinel-2 imagery, with a 30 m spatial resolution. The DSWx-HLS dataset served as the primary reference for NDWI threshold optimization and validation. The JRC Global Surface Water dataset, obtained through GEE, provides a long-term record of monthly surface water observations with a 30 m spatial resolution from 1984 to 2021. JRC Global Surface Water data from 1985 to 2021 were used to match the study period of this project.

Table 1b
Validation Datasets

Platform	Use	Date Range Used in GUI
OPERA Dynamic Surface Water Extent from Harmonized Landsat Sentinel-2 product (DSWx-HLS)	Determine optimized thresholds for NDWI, to classify open water.	2016–2026
JRC Global Surface Water	Determine optimized thresholds for NDWI, to classify open water.	1985–2021
Google Dynamic World Version 1 (DW)	Determine optimized thresholds for NDVI, to classify vegetation.	2015–2026
National Wetland Inventory (NWI)	Determine optimized thresholds for NDMI, to classify wetlands.	1985–2026

For NDVI optimization, we accessed Google Dynamic World Version 1 through GEE to obtain near-real-time, 10 m land cover classifications derived from Sentinel-2 imagery. We used Dynamic World (DW) exclusively to calibrate NDVI thresholds by distinguishing vegetated land cover classes from non-vegetated classes. For NDMI optimization, we accessed the United States Fish and Wildlife Service National Wetland Inventory (NWI), which includes wetland mapping that began in 1974. NWI data from 1985 to 2026 were used to match the study period of this project. The NWI staff complete these maps through photo interpretation of high-resolution images and update them on a project-by-project basis across the United States. Together, these reference datasets provided high-quality observations spanning both historical and contemporary periods, enabling us to calibrate and validate site-specific classification thresholds for Lake Abert and the Great Salt Lake.

2.2 Data Processing

2.2.1 Earth Observation Calculations

The analysis drew on over 40 years of Earth observation imagery acquired between 1985 and 2026, as standardized inputs for lake and wetland classification. We filtered Landsat image collections, as displayed in Table 1a, to the Lake Abert and Great Salt Lake study areas, and produced seasonal composites for each year between 1985 and 2026. We then removed cloud-contaminated pixels using the QA_PIXEL band and converted surface reflectance bands using the standard U.S. Geological Survey (USGS) Collection 2 scaling formula, applying a scale factor of 0.0000275 and an additive offset of -0.2 to each band (U.S. Geological Survey, 2023). Because different Landsat missions assign different band numbers to equivalent spectral regions, we renamed the corresponding bands to a standardized convention to ensure consistent spectral index calculations across sensors. Finally, we merged the processed imagery from all available Landsat missions into a single image collection, followed by generating a pixel-wise median.

The processed imagery was used to calculate spectral indices that characterize vegetation, vegetation water content, and surface moisture. These indices served as inputs for lake and wetland classification, with classification thresholds optimized using a grid search validation approach. Guided by the methodologies of Al-Maliki et al. (2022) and Ashok et al. (2021), we derived the following spectral indices: the Normalized Difference Vegetation Index (NDVI; Equation 1; Kriegler et al., 1969 and Tucker et al., 1979), Normalized Difference Moisture Index (NDMI; Equation 2; Wilson & Sader, 2002), and the Normalized Difference Water Index (NDWI; Equation 3; McFeeters, 1996). In the equations below, NIR represents near-infrared surface reflectance, Red represents red surface reflectance, SWIR represents shortwave infrared surface reflectance, and Green represents green surface reflectance.

$$\mathrm{NDVI} = \frac{\mathrm{NIR} - \mathrm{Red}}{\mathrm{NIR} + \mathrm{Red}} \tag{1}$$

$$\mathrm{NDMI} = \frac{\mathrm{NIR} - \mathrm{SWIR1}}{\mathrm{NIR} + \mathrm{SWIR1}} \tag{2}$$

$$\mathrm{NDWI} = \frac{\mathrm{Green} - \mathrm{NIR}}{\mathrm{Green} + \mathrm{NIR}} \tag{3}$$

2.2.2 Threshold Optimization

For the NDWI and NDVI reference datasets, we temporally matched Landsat scenes to the nearest available reference observation. From each matched scene, we randomly sampled 200-pixel locations at a 30 m resolution, with per-scene random seeding to ensure sampled locations varied from scene to scene. Then, we projected all sample points into a local UTM coordinate system and aggregated them into 1 km x 1 km spatial blocks. A random assignment process split these spatial blocks into training (80%) or test (20%) subsets. This ensured spatial separation between the data used to fit thresholds and the data used to validate them.

The NWI reference dataset offers limited temporal coverage, so we used a single Landsat composite spanning from 2010 to 2020 during the summer months (June to September) for NDMI threshold optimization, chosen to encompass the years in which wetland mapping occurred within the study areas. Before sampling, we masked open water—classified from the NDWI threshold—from the composite, since NDMI otherwise misclassifies open water as wetland. The team then randomly sampled 200-pixel locations from the masked composite, aggregated into the same 1 km spatial blocks, and split into training and test subsets following the procedure described above.

Within the training set, we used a five-fold cross-validation with spatial blocks as the grouping unit to determine each index's optimal threshold. For each fold, we performed a grid search over the candidate threshold range, using the Intersection over Union (IoU; Equation 4) between predicted and reference classification as the selection metric. The best-performing threshold from that fold's training data was then evaluated on the fold's held-out portion. The final threshold for each index is the mean of the five-fold-level thresholds. The mean of the five held-out fold scores provided a cross-validated performance estimate without using the reserved test set.

$$\mathrm{IoU} = \frac{\text{Area of Intersection}}{\text{Area of Union}} \tag{4}$$

2.3 Data Analysis

2.3.1 Statistical Analysis

Threshold optimization relied on four performance metrics: IoU (Equation 4), F1 score (Equation 5), precision (Equation 6), and recall (Equation 7). IoU served as the primary optimization metric because it penalizes false positives (FP) and false negatives (FN) symmetrically and is widely used to assess the accuracy of surface water and land cover classifications (Jaccard, 1912; Liu et al., 2007). F1 score, precision, and recall provided a more comprehensive assessment of classification performance and helped characterize the types of errors associated with each threshold. We reported IoU at two stages of the threshold optimization pipeline. First, we calculated the mean cross-validated IoU across the five validation folds using only the training data. This metric quantified threshold performance during model selection while preventing information from the test set from influencing threshold optimization. After selecting the optimal threshold for each spectral index, we evaluated IoU, F1 score, precision, and recall one time using the independent test dataset. These test-set metrics represent the final, unbiased performance of each index-reference threshold combination. IoU measures the spatial overlap between the predicted and reference classifications. The F1 score is the harmonic mean of precision and recall, where precision represents the proportion of predicted positive pixels that are true positives (TP), and recall represents the proportion of true-positive pixels that are correctly identified.

$$\text{F1 Score} = 2 \times \frac{\text{Precision} \times \text{Recall}}{\text{Precision} + \text{Recall}} \tag{5}$$

$$\text{Precision} = \frac{\mathrm{TP}}{\mathrm{TP} + \mathrm{FP}} \tag{6}$$

$$\text{Recall} = \frac{\mathrm{TP}}{\mathrm{TP} + \mathrm{FN}} \tag{7}$$

2.3.2 QGIS Plugin Creation

We developed the GUI for the plugin in Python using Visual Studio Code, chosen for its accessible setup and strong support for Python development, merging capabilities, and version control. We followed standard QGIS plugin architecture, building the interface as a dock widget that integrates directly into the QGIS window. The plugin can be added and accessed directly from the QGIS plugin menu, facilitating handoffs between users. We organized development around a clear separation between the interface code, which manages the panel layout and user inputs, and the backend code, which handles communication with GEE, such as retrieving imagery and computing spectral indices. Keeping these pieces separate allowed each part to be built independently and ensured the interface could still open even before the user entered a project code and configured a GEE connection. Throughout code development, we loaded and reloaded the plugin within QGIS, allowing changes made in QGIS to be tested immediately within the live QGIS environment. This workflow supported an iterative design process in which the panel layout, user inputs, and backend functionality could be refined by team members and merged to produce an intuitive and valuable tool for lake classification.

2.3.3 Threshold-Based Land Classification

Our threshold-based classification workflow analyzed seasonal spectral index composites and resultantly delineated open water, wetlands, and terrestrial land cover within the chosen study area. Users can select a study area by choosing a pre-selected region (Lake Abert or the Great Salt Lake), loading an AOI from a file upload, or drawing a bounding box on the interactive map. After entering a GEE project code and year, the plugin can be used to fetch true color imagery, LST, NDWI, NDVI, and NDMI as added layers to the map. In addition, users can optionally download seasonal summed OpenET Ensemble Monthly Evapotranspiration 2.0 data (Melton et al., 2021). The QGIS plugin interface allows users to interactively adjust NDWI, NDVI, and NDMI thresholds, or use the provided optimal thresholds as set in the backend. User inputs to the plugin can be found in Figure A1 of Appendix A. The plugin applies these thresholds to each pixel in the multi-index raster to generate a classified land cover map for the selected year (Appendix A, Figure A2). The classification output assigns each pixel to open water, wetland, or land. Open water is identified by pixels equaling or exceeding the optimized NDWI threshold. Wetlands are identified by pixels with NDVI and NDMI values greater than or equal to their respective optimized thresholds, and all remaining pixels are classified as land. This classification approach follows the structure of Al-Maliki et al. (2022), a visual representation of which is displayed in Figure 2. The resulting classified raster is then rendered in QGIS using a standardized color palette to facilitate comparison among queries. The thresholds determined here are default values in the plug-in, and users may easily edit these thresholds manually in the GUI, allowing for applications to other Great Basin terminal lakes or lakes elsewhere.

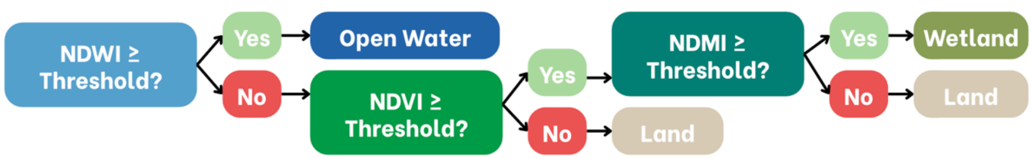

Figure 2: Decision tree for threshold-based land classification.

Following classification and visualization, the plugin computes summary statistics for each land cover class by counting the number of classified pixels and converting these counts to area using the spatial resolution of the Landsat imagery (30 m x 30 m). Class areas are reported in square kilometers together with the proportion of the total classified area represented by each class, and displayed on the GUI user input panel (Appendix A, Figure A1). These quantitative summaries enable users to evaluate lake extent, wetland distribution, and surrounding terrestrial land cover over time. The model also allows the end user to compute a summer (June-September) composite time series graph of lake extent in a chosen year, which is useful for lake extent monitoring over time. An example of this time series can be found in Figure A3 of Appendix A.

3. Results

3.1 Analysis of Results

3.1.1 NDWI Optimized Threshold Results

We selected OPERA as the primary reference dataset for threshold optimization due to its frequent updates and greater availability of current data compared to JRC. To evaluate the resulting NDWI thresholds, we compared classification performance against both reference datasets for the Great Salt Lake and Lake Abert (Table 2). For the Great Salt Lake, the optimized threshold yielded 0.0151 for JRC and -0.055 for OPERA, with an IoU score of 0.870 for JRC and 0.793 for OPERA (Table 3). For Lake Abert, the optimized threshold yielded 0.084 for JRC and −0.063 for OPERA, with an IoU score of 0.844 for JRC and 0.655 for OPERA. While JRC showed higher agreement at both sites, OPERA's classification performance remained strong, supporting its use as the primary threshold dataset given its advantages in temporal resolution and update frequency.

Table 2

Performance Metrics for Threshold Optimization

Site	Index Variable	Threshold	IoU
Great Salt Lake	NDWI – JRC	0.0151	0.870
	NDWI – OPERA	-0.055	0.793
	NDVI	0.165	0.780
	NDMI	0.053	0.092
Lake Abert	NDWI – JRC	0.084	0.844
	NDWI – OPERA	-0.063	0.655
	NDVI	0.130	0.705
	NDMI	0.123	0.216

Table 3

NDWI Threshold Optimization

Site	Reference Dataset	Optimized Threshold	IoU
Great Salt Lake	OPERA	-0.055	0.793
	JRC	0.0151	0.870
Lake Abert	OPERA	-0.063	0.655
	JRC	0.084	0.844

3.1.2 NDVI Optimized Threshold Results

We selected DSWx-HLS dataset to evaluate the grid search-optimized NDVI threshold for the Great Salt Lake and Lake Abert. For the Great Salt Lake, the optimized threshold yielded 0.165 with an IoU score of 0.780 (Table 4). For Lake Abert, the optimized threshold yielded 0.130 with an IoU score of 0.705.

Table 4

NDVI Threshold Optimization

Site	Optimized Threshold	IoU
Great Salt Lake	0.165	0.780
Lake Abert	0.130	0.705

3.1.3 NDMI Optimized Threshold Results

We used the median composite as the primary method for NDMI threshold optimization. We additionally evaluated a 99th percentile composite to assess its ability to capture peak environmental phases, such as periods of maximum moisture. For the Great Salt Lake, the optimized threshold yielded 0.053 for the median composite and 0.356 for the 99th percentile, with IoU scores of 0.092 for the median and 0.085 for the 99th percentile (Table 5). For Lake Abert, the optimized threshold yielded 0.123 for the median composite and 0.407 for the 99th percentile, with IoU scores of 0.216 for the median and 0.423 for the 99th percentile. Additional performance metrics, including F1 scores, precision, and recall, are provided in Tables B1 and B2 of Appendix B: *Optimization Performance Metrics*.

Table 5

NDMI Threshold Optimization

Site	Composite	Optimized Threshold	IoU
Great Salt Lake	Median	0.053	0.092
	99th Percentile	0.356	0.085
Lake Abert	Median	0.123	0.216
	99th Percentile	0.407	0.423

3.1.4 Residual Maps and Confusion Matrices

Figure 3 presents the residual maps and confusion matrices used to evaluate the threshold-based classifications for the Great Salt Lake and Lake Abert. The residual maps identify locations where the threshold classifications differed from the reference datasets, while the confusion matrices summarize the numbers of true positives, true negatives, false positives, and false negatives for each classification. The NDWI classification correctly classified most pixels as either water or non-water, with the majority of errors occurring along shorelines and other transitional boundaries where mixed pixels are common. Similarly, the NDVI confusion matrices indicate high agreement between predicted and reference vegetation classes, with relatively few false-positive classifications. These visual assessments complement the reported IoU, F1, precision, and recall metrics by illustrating the spatial distribution and magnitude of classification errors.

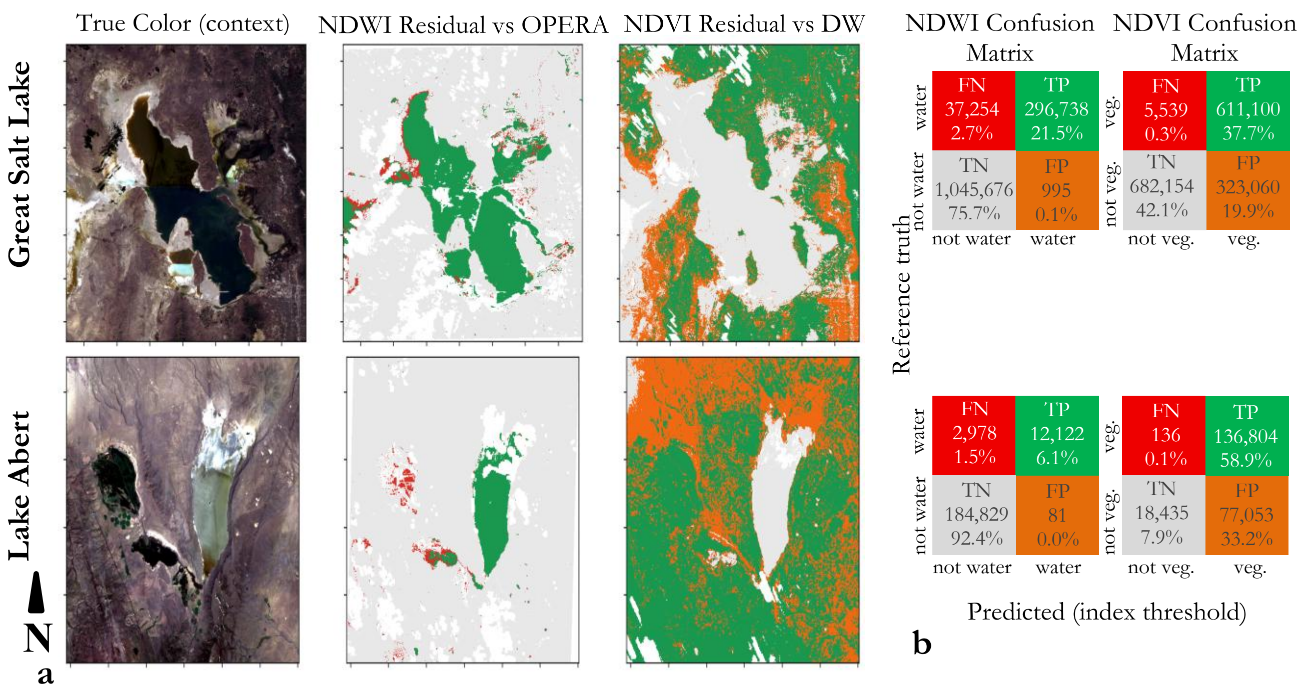

Figure 3: Residual maps, FN: red, TP: green, TN: gray, FP: orange (a) and corresponding confusion matrices (b) highlighting differences between the reference datasets and the threshold-based land classification.

3.1.5 Time Series and Stage-Area Relationships

Figure 4 shows a time series of lake surface areas calculated from the threshold-based classification and lake elevation measured at USGS monitoring stations at each lake. The Great Salt Lake contains two USGS monitoring stations, at the north and south arms of the lake, which have been continuously monitoring the lake's properties since 1999. The two arms are separated by a causeway, and while some water is exchanged through culverts, breaches, and the permeability of the culvert, they function as independent bodies of water. The Lake Abert monitoring station is much newer, having come online in 2023. Due to snow and ice artifacts, we calculated surface water extent only in the period from April through October, and some outliers remain, likely also caused by snow events inside that period. Although Lake Abert shows more fluctuation in lake extent over time, the Great Salt Lake graph depicts a steady decline since 1999 in monthly median water extent based on both reference and tool-derived data.

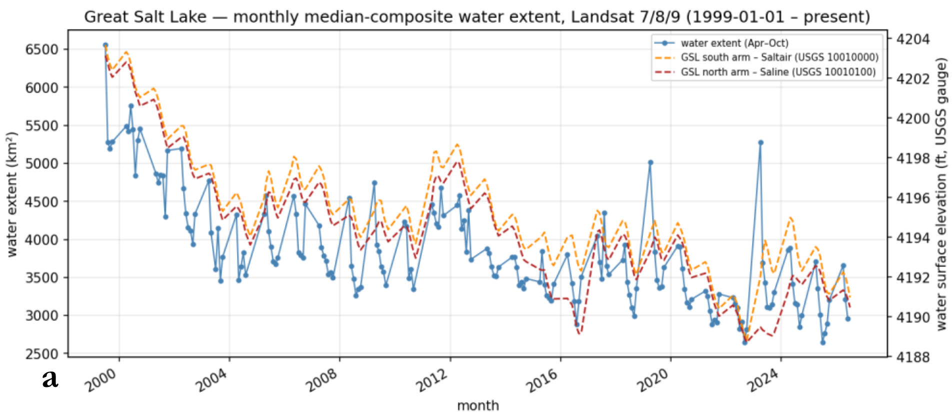

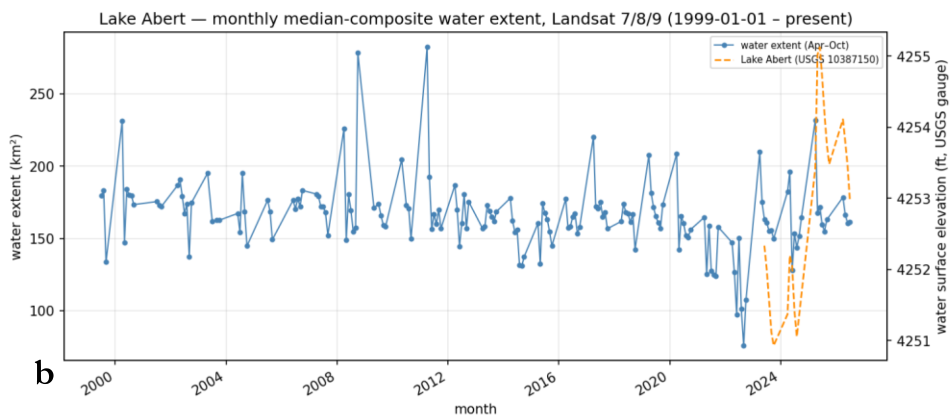

Figure 4: Time series of threshold-derived lake surface area and observed lake stage for the Great Salt Lake (a) and Lake Abert (b). We calculated seasonal lake surface area from the optimized NDWI threshold applied to Landsat imagery between 1985 and 2026 and compared with in-situ lake stage measurements collected at United States Geological Survey (USGS) monitoring stations.

For each monitoring station, we graphed the relationship between threshold-derived surface area and in-situ surface height. As surface elevation and surface height are monotonically, but not linearly, related, we calculated Spearman rank correlation for each relationship. Notice in Figure 5 that because the USGS deployed the monitoring station at Lake Abert much more recently, the sample size (n = 20) is much lower, and the relationship is more difficult to constrain than the Great Salt Lake stations (n = 175). Point colors represent acquisition date, illustrating the long-term decline in both lake stage and surface area over the past decade, followed by a modest recovery beginning around 2023.

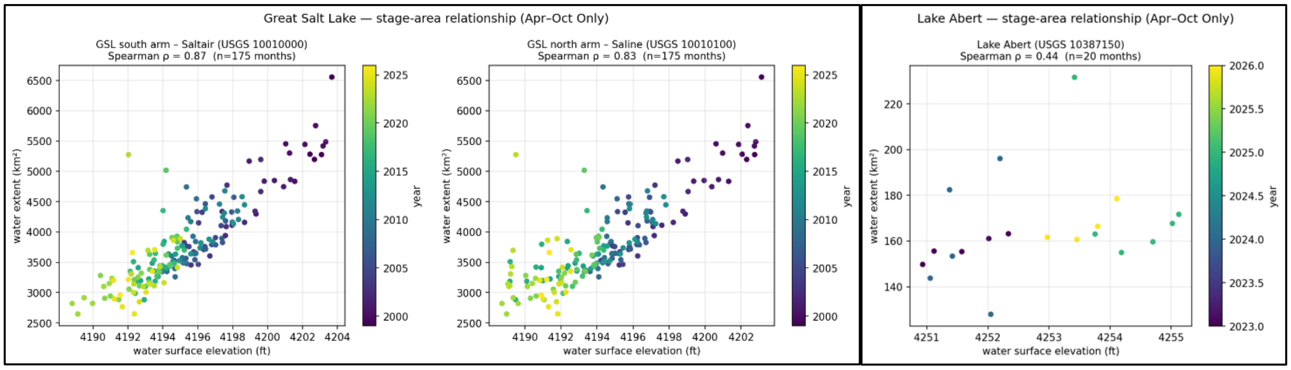

a **b**

Figure 5: Relationship between threshold-derived lake surface area and measured lake stage for the Great Salt Lake (a) and Lake Abert (b). Scatterplots compare Landsat-derived lake surface area generated from the optimized NDWI threshold with concurrent USGS lake stage observations.

3.2 Errors & Uncertainties

Multiple sources of error and uncertainty within the methodology affected the performance of the threshold optimization and the land classification workflow. One source of error is spectral mixing within Landsat's 30 m pixels, where a single pixel may contain multiple land cover types. This can result in the misclassification of land cover within the validation sets. This classification error occurs due to land cover types having similar spectral signatures, making the error especially likely in transitional areas between open water, wetlands, and the surrounding land. A second source of uncertainty is the temporal mismatch between the Landsat imagery and the reference datasets used for determination and validation of the threshold optimization. While the JRC, OPERA, and DW datasets provide high-quality reference information, they are all satellite-derived model outputs rather than field-level ground truth observations. Additionally, the NWI validation dataset, used to optimize the NDMI threshold, is spatially static and updated on a project-by-project basis across the United States rather than at a periodic rate. As a result of these temporal limitations, the NWI may not accurately represent wetland conditions at the time imagery was collected, contributing to the relatively lower NDMI classification performance.

Sensor- and season-related factors also introduced uncertainty. Imagery acquired by Landsat 7 after the 2003 Scan Line Corrector (SLC) failure contained data gaps that may reduce the accuracy of classification despite preprocessing. This is a sensor-level complication and not attributable to gaps in this project's methodology. In addition, winter imagery that contains snow and ice can alter spectral response and interfere with the effectiveness of NDWI for classifying open water, which may lead to increased omission or commission errors. We leveraged the QA_PIXEL mask in the methods to remove cloud-covered pixels, but atmospheric effects and cloud contamination may remain, subsequently influencing values for the chosen indices. Finally, this study used a classification-based approach using NDWI, NDVI, and NDMI. The fixed thresholds for these indices may not fully capture all variability across years and environmental conditions. Future work could improve classification accuracy by incorporating field observations for validation, expanding reference datasets, or evaluating new models or methods for classification.

4. Conclusions

4.1 Interpretation of Results

The results presented in the previous sections demonstrate that a threshold-based remote sensing workflow can effectively monitor long-term changes in terminal lakes using open-access Earth observation data. Classification of open water produced the strongest performance, with NDWI thresholds reaching IoU values of 0.870 and 0.844 for the Great Salt Lake and Lake Abert, respectively, when validated against the JRC dataset. Although OPERA produced slightly lower agreement, it maintained strong classification performance while providing more current observations, making it the most well-suited for consistent monitoring. NDVI also achieved high classification accuracy for vegetation, indicating that vegetation surrounding the lakes can be reliably identified using the threshold-based approach we employed. In contrast, NDMI produced substantially lower accuracy, which highlights the challenges of correctly mapping wetlands using a single spectral index as well as showing the limitations of available wetland reference datasets.

The time-series analyses further demonstrate that the threshold-derived lake extents closely follow observed changes in lake elevation, indicating that the methodology captures meaningful long-term hydrologic trends. The stage-area analysis also validates the classification approach by demonstrating a consistent relationship between remotely sensed lake extent and in-situ water level measurements. The results show that Earth observations can provide a consistent record of saline lake decline spanning more than four decades, allowing resource managers to evaluate how specified lakes respond to changing climate and water use over time.

4.2 Partner Implementation

Monitoring the Great Basin Lakes currently relies heavily on field surveys and manual GIS analyses that are time-consuming, expensive, and require specialized expertise. The GIS plug-in developed through this project makes long-term monitoring of under-resourced lakes more efficient and easily accessible. The plug-in is a user-friendly mapping tool that can be used to analyze historical lake and wetland extent from June to September from 1985 through 2026, drawing on decades of satellite imagery archives (Figure 6). Rather than requiring users to manually locate, download, and preprocess raw satellite data, the tool automates these steps into a streamlined workflow accessible through an open-access mapping interface.

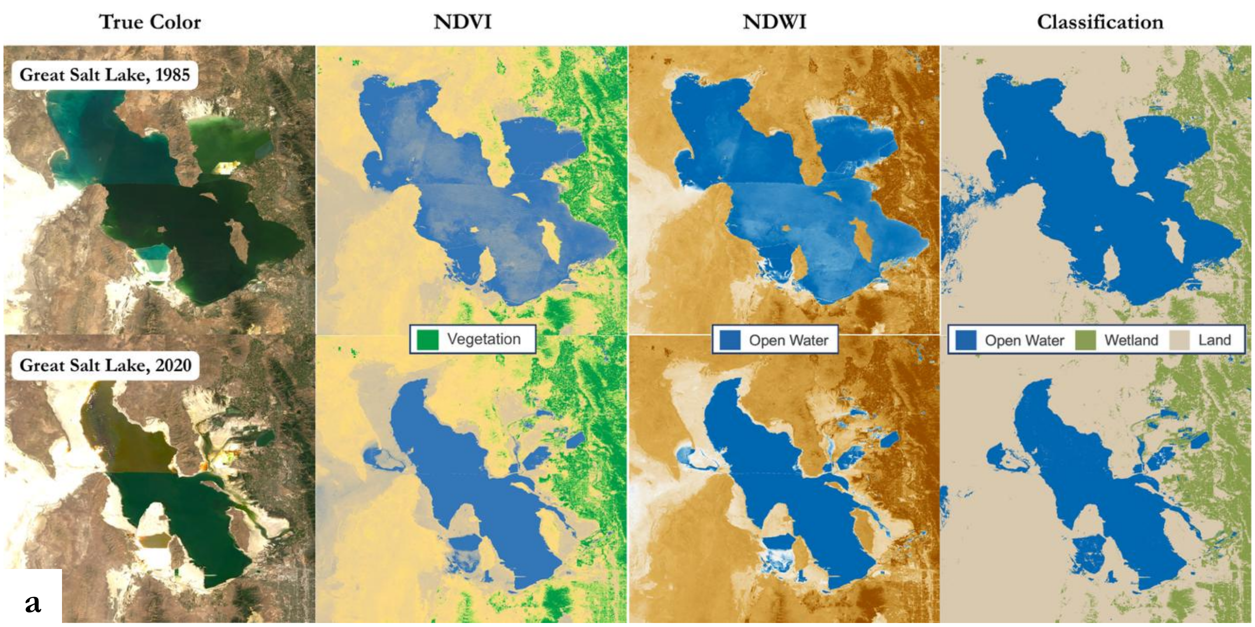

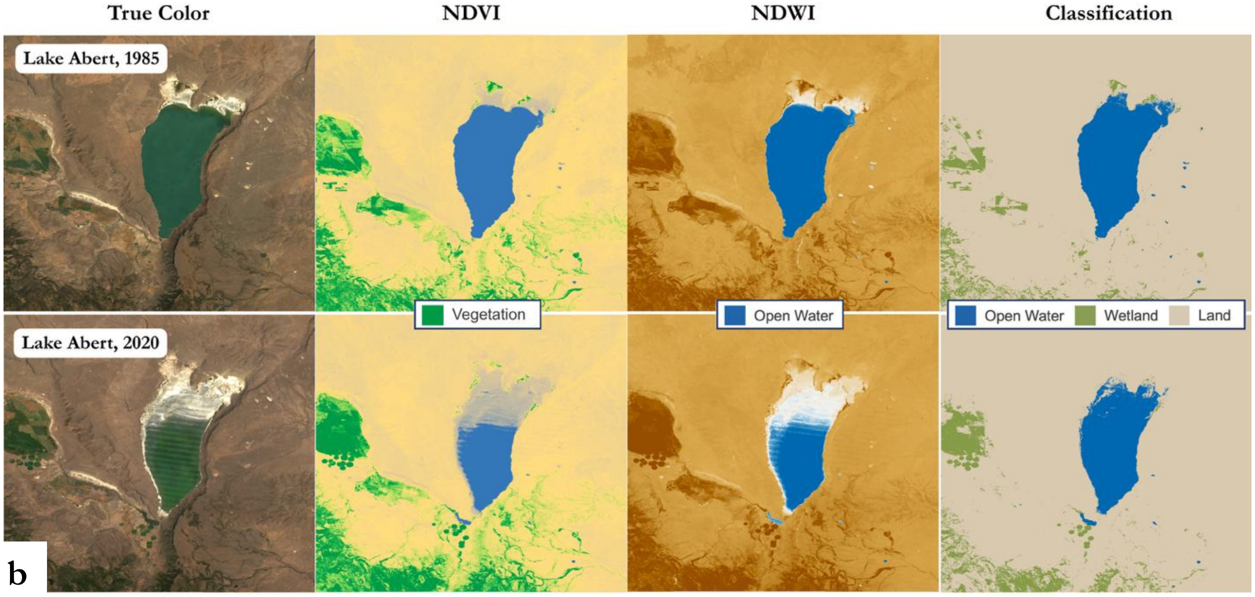

Figure 6: Comparison of Earth observation products generated by the QGIS plugin for the Great Salt Lake (a) and Lake Abert (b) during 1985 and 2026. For each study area, the plugin produces true-color imagery, NDVI, NDWI, and threshold-based land classifications of open water, wetlands, and terrestrial land cover. The side-by-side comparison illustrates long-term changes in lake extent and surrounding vegetation while demonstrating the standardized outputs generated through the automated plugin workflow.

Users can define an area of interest in three ways: by selecting one of the pre-assigned lakes (Lake Abert or Great Salt Lake), directly selecting a region on a map, or by uploading a boundary file (e.g., shapefile) for a specific site. The tool then processes the relevant imagery and returns classified imagery based on the user's indices outputs within the selected time range. This streamlined workflow allows partners to track change over nearly four decades without needing remote sensing expertise. We initially developed the plug-in tool for the Great Salt Lake, UT, and Lake Abert, OR as pilot sites, both of which face well-documented water level declines and ecological stress. However, we intentionally built the underlying workflow for adaptability, so partners can extend the tool to other underserved or under-monitored lakes across the Great Basin. This design choice ensures the tool's utility extends beyond its original pilot sites and can scale as monitoring needs grow across the region.

By lowering the technical and financial barriers to long-term monitoring, the GUI enables ODWR and UDWR to make more timely, informed conservation and water management decisions. ODWR emphasized that stakeholders, like farmers, environmentalists, and wildlife groups, often struggle to communicate data across groups with different priorities and expertise. This tool offers them an efficient way to share findings and convey how sensitive these lakes' resources are to surrounding communities. The GUI will serve as a baseline for future scientific research by the partners and universities in the coming years. UDWR stated the GUI can support future work such as invasive species classification in wetlands, evapotranspiration rate estimation, and identification of key predictors for wetland detection using satellite imagery.

The code required for the plugin is hosted in a GitHub repository to ease the transition to the project partners. The team also created a tutorial for download, setup, installation, and use of the plugin with QGIS. Future development could improve wetland classification by incorporating machine learning algorithms and higher-resolution imagery, such as Sentinel-2, while integrating additional environmental datasets to enhance monitoring capabilities. The plugin could further be expanded to include quarterly seasonal compositing rather than solely annual summer composites.

5. Acknowledgements

We would like to thank the following individuals for their essential guidance, collaboration, and support throughout this project:

- **Timothy Mayer –** NASA Marshall Space Flight Center, University of Alabama in Huntsville
- **Sean Fleming –** NASA Ames Research Center, California State University Monterey Bay
- **Jeremy Rapp –** NASA Marshall Space Flight Center, University of Alabama in Huntsville
- **Kaylee Tanner –** Utah Department of Natural Resources, Division of Water Resources
- **Craig Miller –** Utah Department of Natural Resources, Division of Water Resources
- **Mahmud Aveek –** Utah Department of Natural Resources, Division of Water Resources
- **Graham Thomas –** Oregon Department of Water Resources
- **Caiden Hartrich –** Analytical Mechanics Associates

This material contains modified Copernicus Sentinel data (2016–2026), processed by ESA.

Any opinions, findings, and conclusions or recommendations expressed in this material are those of the authors and do not necessarily reflect the views of the National Aeronautics and Space Administration.

This material is based upon work supported by NASA through contract 80LARC23DA003.

6. References

Akumu, C. E., Pathirana, S., Baban, S., & Bucher, D. (2010). Monitoring coastal wetland communities in north-eastern NSW using ASTER and Landsat satellite data. *Wetlands Ecology and Management*, *18*(3), 357–365. https://doi.org/10.1007/s11273-010-9176-0.

Al-Maliki, S., Ibrahim, T. I. M., Jakab, G., Masoudi, M., Makki, J. S., & Vekerdy, Z. (2022). An approach for monitoring and classifying marshlands using multispectral remote sensing imagery in arid and semi-arid regions. *Water*, *14*(10), 1523. https://doi.org/10.3390/w14101523.

Ashok, A., Rani, H. P., & Jayakumar, K. V. (2021). Monitoring of dynamic wetland changes using NDVI and NDWI based landsat imagery. *Remote Sensing Applications: Society and Environment*, *23*, 100547. https://doi.org/10.1016/j.rsase.2021.100547.

Frus, R. J., Aldridge, C. L., Casazza, M. L., Eagles-Smith, C., Herring, G., Hynek, S. A., Jones, D. K., Kemp, S. K., Marston, T. M., Morris, C. M., Naranjo, R. C., Nell, C. S., O'Leary, D. R., Overton, C. T., Pulver, B. A., Reichert, B. E., Rumsey, C. A., Schuster, R., & Smith, C. D. (2023). *Integrated science strategy for assessing and monitoring water availability and migratory birds for terminal lakes across the Great Basin, United States* (No. 1516). U.S. Geological Survey. https://doi.org/10.3133/cir1516.

Hall, D. K., Kimball, J. S., Larson, R., DiGirolamo, N. E., Casey, K. A., & Hulley, G. (2023). Intensified warming and aridity accelerate terminal lake desiccation in the Great Basin of the Western United States. *Earth and Space Science*, *10*(1). https://doi.org/10.1029/2022EA002630.

Herring, G., Whipple, A. L., Aldridge, C. L., Pulver, B. A., Eagles-Smith, C. A., Inman, R. D., Matchett, E. L., Monroe, A. P., Orning, E. K., Robb, B. S., Shyvers, J. E., Tarbox, B. C., Van Schmidt, N. D., Smith, C. D., Holloran, M. J., Overton, C. T., O'Leary, D. R., Casazza, M. L., & Frus, R. J. (2025). Imperiled Great Basin terminal lakes: Synthesizing ecological and hydrological science gaps and research needs for waterbird conservation. *BioScience*, *75*(2), 112–126. https://doi.org/10.1093/biosci/biae126.

Jaccard, P. (1912). The Distribution of the Flora in the Alpine Zone. *New Phytologist*, *11*(2), 37–50. https://doi.org/10.1111/j.1469-8137.1912.tb05611.x.

Kriegler, F., Malila, W., Nalepka, R., & Richardson, W. (1969). Preprocessing Transformations and Their Effects on Multispectral Recognition. https://www.semanticscholar.org/paper/Preprocessing-Transformations-and-Their-Effects-on-Kriegler-Malila/aa0f092bba168a62cc913d027a4a892cac3e8e94.

Landsat Collection 2 Surface Reflectance (2023). *U.S. Geological Survey*. https://www.usgs.gov/landsat-missions/landsat-collection-2-surface-reflectance.

Liu, C., Frazier, P., & Kumar, L. (2007). Comparative assessment of the measures of thematic classification accuracy. *Remote sensing of environment*, 107(4), 606-616. https://doi.org/10.1016/j.rse.2006.10.010.

Melton, F., Huntington, J., Grimm, R., Herring, J., Hall, M., Rollison, D., Erickson, T., Allen, R., Anderson, M., Fisher, J., Kilic, A., Senay, G., volk, J., Hain, C., Johnson, L., Ruhoff, A., Blankenau, P., Bromley, M., Carrara, W., Daudert, B., Doherty, C., Dunkerly, C., Friedrichs, M., Guzman, A., Halverson, G., Hansen, J., Harding, J., Kang, Y., Ketchum, D., Minor, B., Morton, C., Revelle, P., Ortega-Salazar, S., Ott, T., Ozdogon, M., Schull, M., Wang, T., Yang, Y., Anderson, R. (2021). OpenET: Filling a Critical Data Gap in Water Management for the Western United States. *Journal of the American Water Resources Association,* 58(6), 971-994. doi:10.1111/1752-1688.12956.

McFeeters, S. K. (1996). The use of the Normalized Difference Water Index (NDWI) in the delineation of open water features. *International Journal of Remote Sensing,* 17(7), 1425–1432. https://doi.org/10.1080/01431169608948714.

Moore, J. N. (2016). Recent desiccation of Western Great Basin Saline Lakes: Lessons from Lake Abert, Oregon, U.S.A. *Science of The Total Environment*, *554–555*, 142–154. https://doi.org/10.1016/j.scitotenv.2016.02.161.

OPERA (2023). OPERA Dynamic Surface Water Extent from Harmonized Landsat Sentinel-2 (Version 1). *Ver. 1.0. PO. DAAC, CA, USA.* https://doi.org/10.5067/OPDSW-PL3V1.

Tucker, C. J. (1979). Red and photographic infrared linear combinations for monitoring vegetation. *Remote sensing of Environment*, 8(2), 127-150.

United States Fish and Wildlife Service. (2026). *National Wetlands Inventory*. https://doi.org/10.7944/usfws.nwi.202605.

Wilson, E. H., & Sader, S. A. (2002). Detection of forest harvest type using multiple dates of Landsat TM imagery. *Remote Sensing of Environment,* 80(3), 385–396. https://doi.org/10.1016/S0034-4257(01)00318-2.

World Resources Institute & Google. (2022). *Dynamic World V1 near-real-time global 10m land use land cover.* https://developers.google.com/earth-engine/datasets/catalog/GOOGLE_DYNAMICWORLD_V1.

Yulianto, F., Kushardono, D., Budhiman, S., Nugroho, G., Chulafak, G. A., Dewi, E. K., & Pambudi, A. I. (2022). Evaluation of the Threshold for an Improved Surface Water Extraction Index Using Optical Remote Sensing Data. *The Scientific World Journal*, *2022*(1), 4894929. https://doi.org/10.1155/2022/4894929.

7. Appendices

Appendix A: *QGIS Plugin Graphical User Interface (GUI)*

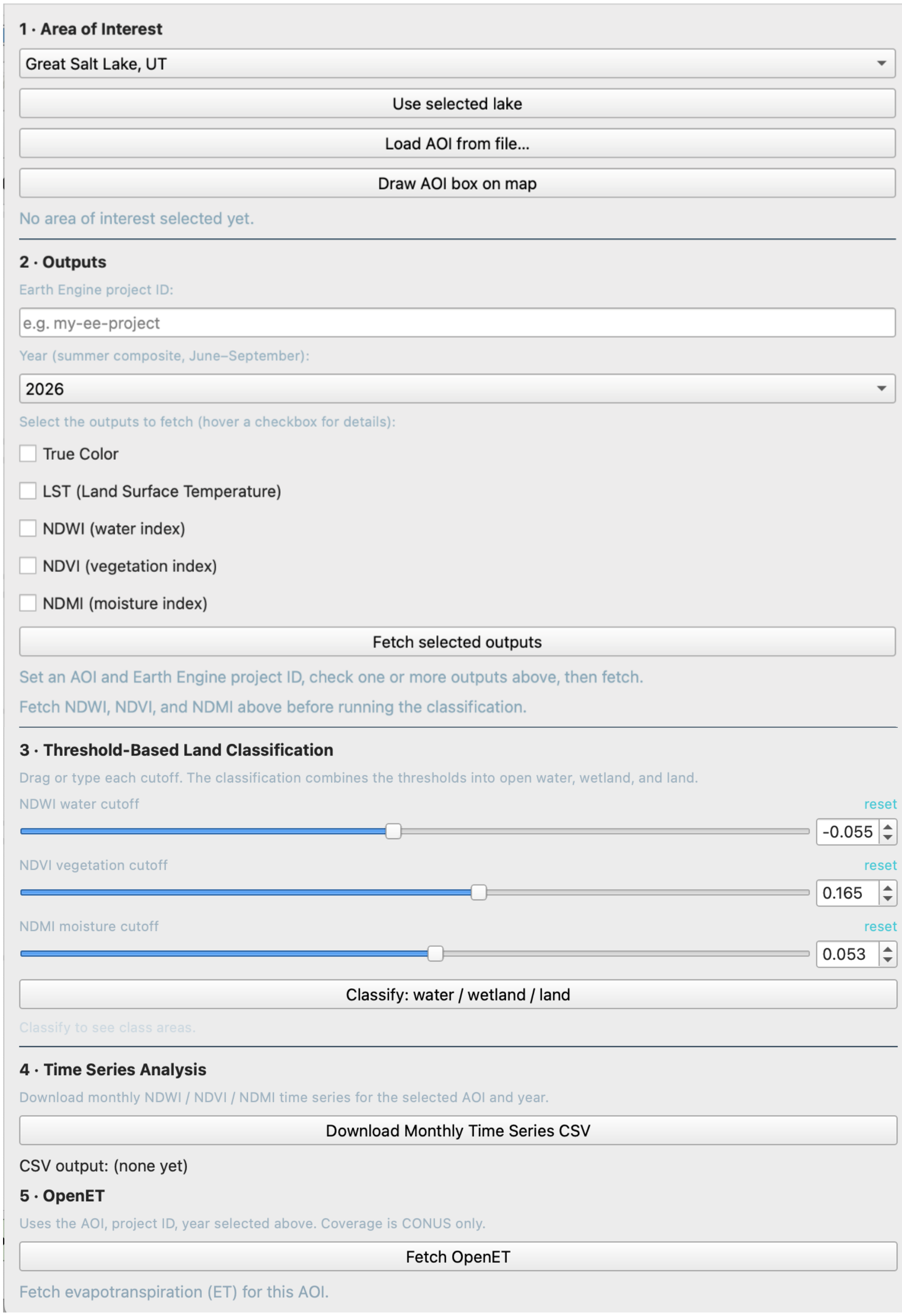

Figure A1. User Inputs to Plugin

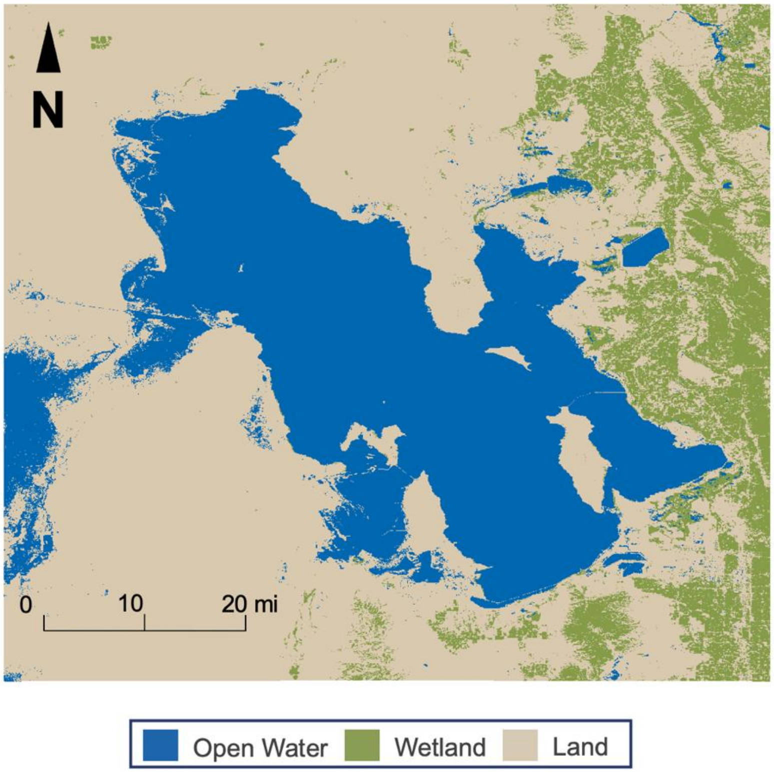

Figure A2. Sample Lake Classification (Great Salt Lake, 2001)

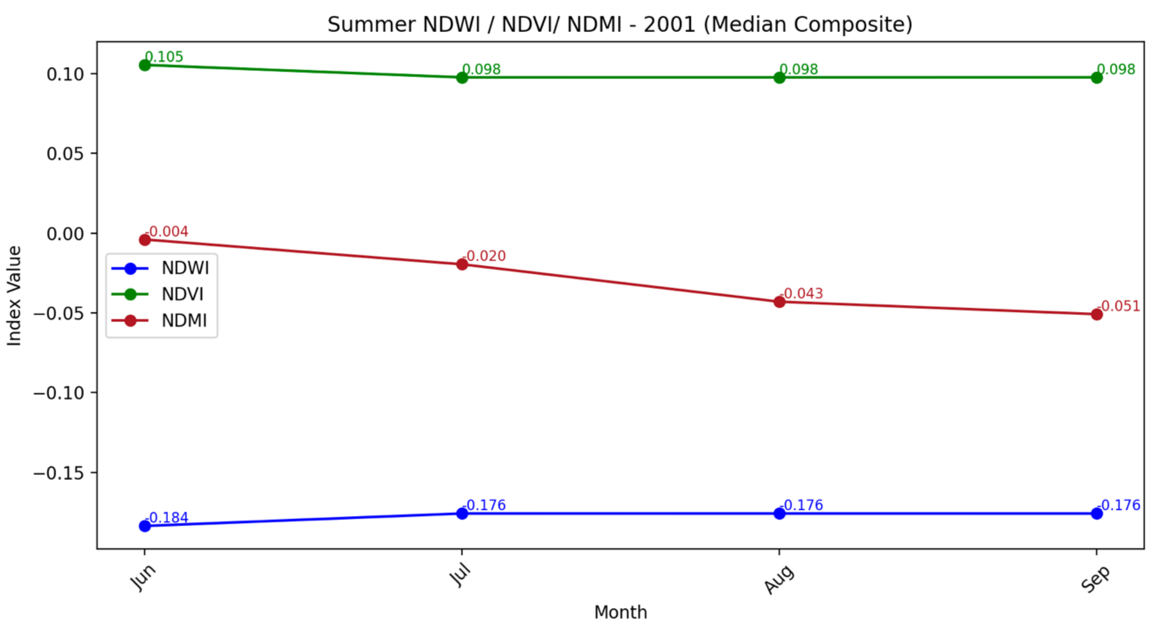

Figure A3. Sample Time Series CSV (Great Salt Lake, 2001)

Appendix B: *Optimization Performance Metrics*

Table B1
Great Salt Lake results

Index Variable	*F1*	*Precision*	*Recall*
NDWI – JRC	0.931	0.953	0.909
NDWI – OPERA	0.885	0.958	0.821
NDVI	0.877	0.790	0.985
NDMI – 99th Percentile	0.156	0.093	0.484
NDMI – Median	0.169	0.100	0.548

Table B2
Lake Abert results

Index Variable	*F1*	*Precision*	*Recall*
NDWI – JRC	0.915	0.977	0.861
NDWI – OPERA	0.792	0.905	0.704
NDVI	0.827	0.712	0.987
NDMI – 99th Percentile	0.635	0.656	0.615
NDMI – Median	0.355	0.329	0.385